

Title of research (EQC grant reference number):

***Rapid, cost-effective 3D monitoring of urban landslide displacements
using UAV-Structure from Motion (SfM)
(3714483)***

Principal Investigator/s, Organisation/s:

Martin Brook, Jon Tunncliffe, University of Auckland

Research team:

*University of Auckland students Jesse Merkle, Vivek Vaidya and Kathryn Ryder undertook fieldwork and data modelling; technician Brendan Hall assisted with UAV data acquisition
Ross Roberts (Auckland Council) provided conceptual ideas and advice at the start of this project*

Key words

Landslide; structure-from-motion; slope stability; Auckland

Summary

The undulating topography of the Auckland urban region is susceptible to landslides of varying process-mechanisms, including: (1) earthflows of saturated Pleistocene Tauranga Group sediments, tephra and residual soils flowing off more competent underlying rock; (2) rotational slumping of man-made fill or Tauranga Group sediments; (3) block-slides of weak Miocene Waitemata Group sedimentary rock, dipping out of slope. Such landslides are often triggered by intense short periods, or prolonged periods of rainfall, such as the 'Tasman Tempest' and ex-Tropical Cyclone Debbie storms of 2017. Typically, rainfall infiltration results in a rise of the groundwater table and an increase of the pore water pressure, causing a reduction in effective normal stress and thereby soil strength, leading to landslides. Such landslide risk is likely to be accentuated in the Auckland region in future given the projected population growth and planned urban and commercial expansion driving the Auckland Unitary Plan (AUP). Indeed, the AUP encourages greater intensification by rezoning many areas to allow construction of low-rise apartments. Therefore, monitoring slope stability in the Auckland region is important, and requires assessment of the extent, rate of displacement, surface topography, and detection of tension cracks developing from slope deformation. Here, we present 10 monitoring investigations of slope failure mechanisms and activity in the Auckland region using Unmanned Aerial Vehicles (UAV) and structure-from-motion (SfM) photogrammetry, as well as some COSI-Corr surface feature tracking trials. UAVs are emerging as an effective tool in landslide hazard management, allowing rapid collection of imagery and production of high resolution photomosaics from which safe evaluation of landslide deformation and activity can be undertaken. In addition, digital terrain models (DTMs) can be developed, and these can potentially allow time-series DTM-differencing and/or comparison with LiDAR data in order to evaluate landslide activity. UAV-derived topographic data is also useful for 2D/3D slope profile construction which is important for accurate parameterization of numerical slope stability models. Thus, the UAV-SfM technique represents an effective, rapid, financially viable alternative to traditional topographic surveying and LiDAR. COSI-Corr showed promise in detecting surface changes, but requires time-consuming manual adjustments to be successful.

1. Introduction

Landslide risk can also be likely accentuated by population growth and the construction expansion driven by the Auckland Unitary Plan (AUP). Across the Auckland region, evidence of slow slope deformation (i.e. cm per year) can be identified. The active Kepa Road landslide within the Pourewa Landslide Zone (PLZ) is a prominent example (Brook & Merkle, 2019).

1.1 UAV-SfM

UAVs can be an effective tool for landslide hazard management due to their ability for (1) rapid high-resolution image collection, (2) production of accurate high-resolution photomosaics, and (3) safe remote evaluation of landslide deformation (Brook & Merkle, 2019). UAVs combined with Structure-from-Motion (SfM) photogrammetry have emerged as a new approach in recent studies for landslide monitoring. The efficiency of SfM algorithms has been demonstrated in multiple studies for landslide monitoring (e.g. Lucieer et al., 2014).

1.2 Objectives

The main objectives of this research will be to:

1. To produce high-resolution 3D point-cloud models, Digital Surface Models (DSMs), Digital Terrain Models (DTMs), and photomosaics using software packages like Pix4DMapper and ArcGIS.
2. Conduct a DEM-Differencing analysis from the generated models to assess any temporal changes in slope displacement across the selected sites in this research.
3. Use the COSI-Corr method at selected sites to further investigate surface movement and feature detection for landslide monitoring.
4. Provide a comprehensive evaluation on the use of the Structure-from-Motion technique for landslide monitoring through the application of UAVs in the Auckland region.

2. Landslides

2.1 Definition

A landslide is defined as the downslope movement of materials such as rock, debris or earth under the influence of gravity. While gravity is the primary driving force for landslide occurrence, other factors affect slope stability that produce specific conditions that make a slope prone to failure, such as rainfall triggering or seismicity (Hungr et al., 2014). Rainfall triggering, in particular, is an issue in Auckland (Brook, 2018). Landslides can occur via a range of processes, at differing rates and on a variety of materials, but development usually follows four subsequent stages of failure (Table 1).

Table 1: Stages of landslide failure (modified from Rotaru et al., 2007).

Stages of Failure	
Stage:	Description:
Pre-failure	Slope surface starts showing evidence of soil creep. Slope mass would be homogeneous and relatively stable.
Failure	Slope failure of the soil/rock is initiated, creating a continuous shear surface.
Post-failure	Soil/rock mass would have active progression after the initial failure has ceased.
Reactivation	Phase of reactivation, where soil/rock mass would fail along one or multiple pre-existing shear faces.

2.3 Landslide classifications

In 1978, Varnes developed a comprehensive and widely utilized classification scheme which became popular in North America. Later modifications to the scheme were also developed (Hung et al., 2014). Varnes (1978) classification scheme included two main variables: (1) the type of landslide movement, and (2) the material type, and from this, 29 types of landslide were suggested (Table 2).

Within the Varnes (1978) framework, the table shows a matrix whose rows represent the type of movement and columns the type of material. This then, provides for 29 landslide type names or keywords, which are further defined and described in the text of his paper. A velocity scale, later updated by International Geotechnical Society's UNESCO Working Party on World Landslide Inventory (WP/WLI) (1995) and Cruden and Varnes (1996) completes the classification (Table 3). For the Auckland region, the velocity scale is of particular importance. This is because landslides can creep at very low velocities (mm/year), unlike in the Southern Alps, where large rock avalanches can occur with rapid velocities (several meters per second).

Table 2: A summary of Varnes' (1978) landslide classification system (from Hung et al., 2014).

Movement type	Rock	Debris	Earth
Fall	1. Rock fall	2. Debris fall	3. Earth fall
Topple	4. Rock topple	5. Debris topple	6. Earth topple
Rotational sliding	7. Rock slump	8. Debris slump	9. Earth slump
Translational sliding	10. Block slide	11. Debris slide	12. Earth slide
Lateral spreading	13. Rock spread	–	14. Earth spread
Flow	15. Rock creep	16. Talus flow	21. Dry sand flow
		17. Debris flow	22. Wet sand flow
		18. Debris avalanche	23. Quick clay flow
		19. Solifluction	24. Earth flow
		20. Soil creep	25. Rapid earth flow
Complex	27. Rock slide-debris avalanche		26. Loess flow
		28. Cambering, valley bulging	29. Earth slump-earth flow

Table 3: Landslide velocity scale from Hungr et al. (2014).

Velocity class	Description	Velocity (mm/s)	Typical velocity	Response ^a
7	Extremely rapid	5×10^3	5 m/s	Nil
6	Very rapid	5×10^1	3 m/min	Nil
5	Rapid	5×10^{-1}	1.8 m/h	Evacuation
4	Moderate	5×10^{-3}	13 m/month	Evacuation
3	Slow	5×10^{-5}	1.6 m/year	Maintenance
2	Very slow	5×10^{-7}	16 mm/year	Maintenance
1	Extremely Slow			Nil

^aBased on Hungr (1981)

Landslide velocity can be attributed to the manner by which a landslide may fail. Slow to very slow velocities can be correlated to ductile failures such as earthflows. In comparison, rapid to extremely rapid velocities are likely associated with instantaneous brittle failures like rockfalls or toppling (Hungr et al., 2014). The velocity of landslide mass movements will determine its damage potential Hungr (2014), however, this will depend on the failure mode, total volume, and estimated depth of the landslide (Sarkar et al., 2015).

New Zealand is susceptible to all landslide classifications mentioned in this sub-section, as a result of its varied geology and climate. Accurately detailed records from New Zealand's database show: (1) translational slides with 1843 occurrences, (2) rotational slumps with 504 occurrences, and (3) flows with 230 occurrences as the most common form of failures throughout the country (Rosser et al., 2017). Although detailed records for the Auckland region are minimal, slow landslide deformations are common. Failures like rotational slumps, block slides and earthflows do occur in the region as seen in published studies (e.g. Brook & Merkle, 2019).

3. Study Area

3.1 Introduction

Sites were chosen across a range of geology and soils, and therefore providing scope for a range of possible failure rates and mechanisms. The geological units in the region include: (1) the Mesozoic Waipapa Terrane greywacke, (2) Early Miocene Waitemata Group sediments (including the East Coast Bays Formation, ECBF), (3) the Pleistocene Tauranga Group sediments and (4) the Auckland Volcanic Field (AVF). The ten landslides surveyed and monitored in this report are sited on Waipapa Terrane residual soils, East Coast Bays formation residual soils, and Tauranga Group sediments.

Multiple trial UAV surveys were undertaken from early 2018 onwards aimed at selecting suitable sites that showed signs of recent/ongoing failure and were accessible. Then, during 2019, two UAV surveys were flown across a five-month time interval at ten chosen landslides. Six of these landslides were selected in Orakei, central Auckland, while the remaining four sites were located across Auckland's eastern coastline,

including two landslides at Kawakawa Bay, and another two at Orere Point (Fig. 1). The first of the 2019 surveys occurred in July, and the second in November, 2019.



Fig. 1: The 3 general site locations selected for study.

3.2 Orakei

Sites 1A-1F for this study are positioned along Kepa Road in Orakei, approximately 4.5 km east of the Auckland CBD (Fig. 2), along the NE side of Orakei Basin, overlooking Pourewa Creek (Fig. 2). Sites 1A-1F are located within the “Pourewa Landslide Zone” (PLZ) which is a zone of slope instability. This zone includes four prehistoric landslides on which the sites have been selected. The Ngapipi Road Landslide (not a focus of this study) is situated at the westernmost corner of Kepa Road. The next sites extending east include: the Kepa Road Landslide (1A-1B), St Joseph’s Landslide (1C-1D), and the Pourewa Landslide (sites 1E-1F).



Fig. 2: The 6 landslides surveyed at Orakei.

Sites 1A-1B extend vertically by approximately 82 m and 151 m respectively from their head-scarp to the Kepa Road fence boundary. Site 1C extends approximately 310 m vertically from its channel head to the shore platform towards Pourewa Creek. Site 1D extends approximately 180 m vertically from its head-scarp down towards its toe. Finally, Sites 1E-1F extend approximately 172 m and 246 m vertically from their head-scarps to their toe regions. Ongoing slope deformation within the PLZ includes shallow retrogressive failures present in the upper slope regions, and translational and flow movements concentrated towards the toe. Tension cracks are also evident along road surfaces at Kepa Road and Ngaio Road, suggesting that ongoing movement is occurring. Underlying most of Orakei is the Early Miocene, East Coast Bays Formation (Edbrooke, 2001). Late Quaternary AVF volcanics (part of the Kerikeri Volcanics Group) is also present at the site. These largely comprise tephra derived from a phreatomagmatic eruption within the Orakei Basin around 85,000 years BP (Nemeth et al., 2012). With the creation of the maar, widespread tuff deposition produced a tuff ring approximately 6-35 m thick covering most of the slopes in the region. This tuff consists of basaltic fragments, ash and lapilli deposits. Holocene landslide deposits comprised of tuff debris and residual ECBF soils also are present.

3.3 Clevedon-Kawakawa Bay Road, Kawakawa Bay

Located approximately 55 km south-east of the Auckland CBD, sites 2A and 2B are situated along the north-western hill slopes of Turei Hill, Kawakawa Bay (Fig. 3). These study sites are characterised by an undulating topography, with the wider Kawakawa bay region showing widespread surface deformation. This is particularly evident at Turei Hill where shallow soil slips and widespread earthflows are common. This deformation has resulted in widespread slope instability, affecting over 1500 residents within the beachfront community.

Historical slope failure has significantly affected the Kawakawa Bay region. Turei Hill most notably has experienced slope instability previously, as documented by previous studies (e.g. Faulkner & Saunders, 2008). The winter months of July-August, 2008, brought an influx of extreme rainfall across the North Island. This triggered a major landslide event across the eastern slope face of Turei Hill. Approximately 300-400 m³ of slip debris consisting of fractured Waipapa Group rock and residual soil failed onto the Clevedon-Kawakawa Bay Road (Faulkner & Saunders, 2008). This debris blockage led to the temporary isolation of the seaside community, consequently having an adverse impact on the local economy (Faulkner & Saunders, 2008), and a much larger, creeping failure of 150,000-250,000 m³ was identified at that time and remediated at a cost of \$4.25 million. Further tension cracks have been mapped on the hill in 2017 (Brook & Merkel, 2019).

Waipapa Group dominates Turei Hill. These rocks are highly weathered and produce weak soil and rock material. The exposed soils across Turei Hill are silty clay in nature and overlay much of the underlying weathered Waipapa Group.

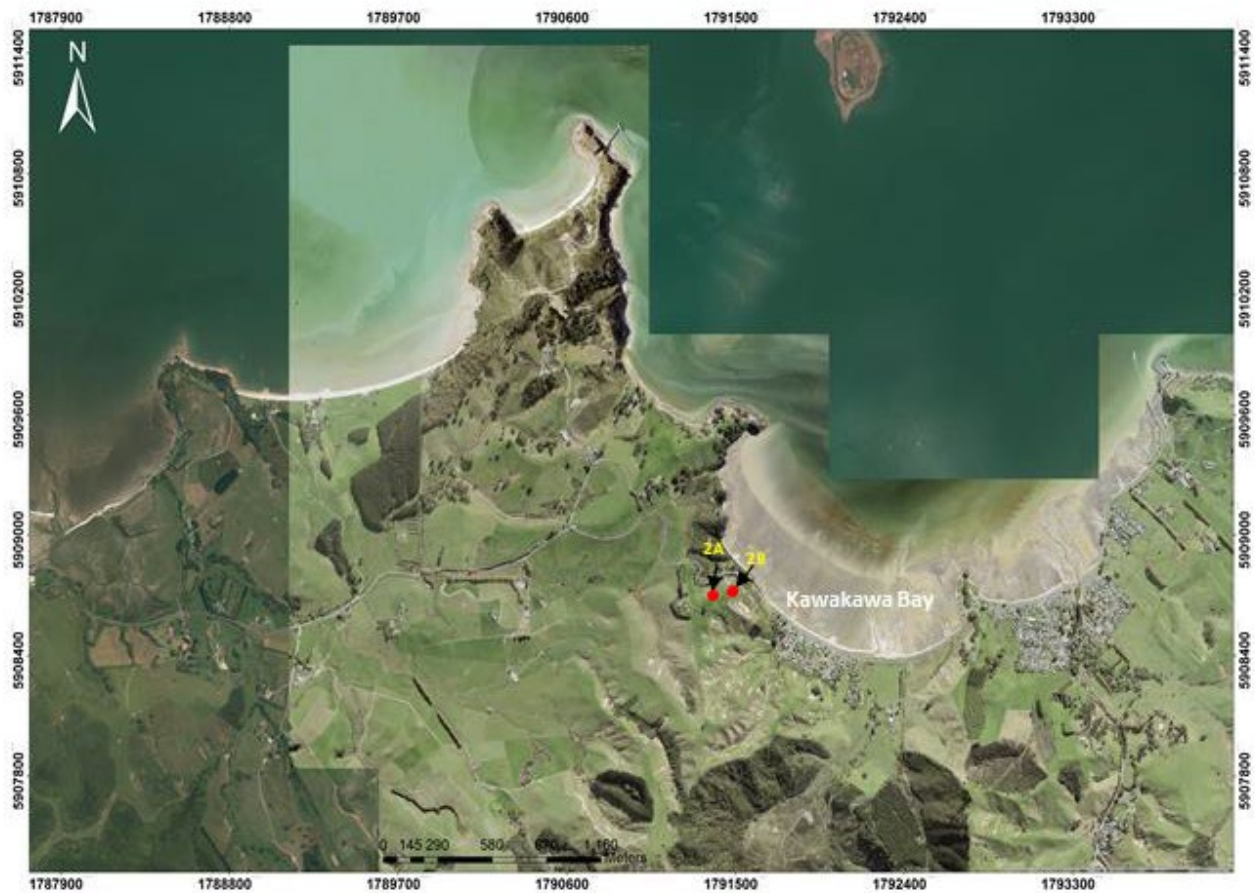


Fig. 3: Location of sites 2A and 2B at Kawakawa Bay.

3.4 Orere Point

The sites 3A and 3B are located along the coastal region of Orere Point, in the coastal cliffs. This a moderately populated rural residential zone follows the extent of the cliff line. Residential properties within this zone are located only meters from the cliff line and head-scarps and are at high risk from slope instabilities. As per Auckland Council guidelines, zones like this are classified as H2 coastal settlement zones under the Auckland Unitary Plan. Cliff heights vary between 20-35 m, present at the eastern and western extents and between 40-50 m towards the centre. Due to their heterogenous nature, the cliffs around Orere Point display variable slope angles. Ryder (2019) suggests that the slope angle is dependent on the lithological characteristics of the cliff and its current geomorphic state (i.e. characteristics of slope failure if it exists).

Sites 3A and 3B at Beach Reserve, Orere Point, have a combined horizontal length of approximately 124 m. Their individual vertical heights vary at 43 and 45 m for 3A and 3B, respectively (Fig. 4). Surface exposure appears greater for site 3A compared to 3B, which has approximately 80-90% vegetation cover. Site geology is mainly alluvially-derived Tauranga Group deposits, overlying Waipapa Group, which outcrops as shore platform and cliff in the west of the bay. Slope deformation at Orere Point has been observed since the 1960s. An increase in slope movement was seen in the 1980s which was subsequently reduced considerably due to slope vegetation stabilisation. Slope deformation has been on the increase since the late 1980s, with periods of slip reactivation which had become more prevalent by 2013 (O'Brien, 2019).

Across sites 3A and 3B, both rotational and planar failures are evident, extending vertically from their head-scarp to the beachfront.



Fig. 4: Location of sites 3A and 3B at Orere Point.

4. Methods

The UAV systems and conducted flight acquisition for UAV-SfM temporal analysis will then be analysed. The SfM workflow used for 3D point cloud modelling and the generation of (1) Digital Surface Models (DSMs) and (2) Digital Terrain Models (DTMs) will then be explored, along with the 2D production of photomosaics. A COSI-Corr assessment will be trialled at selected sites, followed by DEM-differencing for topographic surface change. The differencing will use existing LiDAR data for each site location and compare it with collected UAV-SfM surveys for the temporal change focus of this study.

4.1 GNSS Survey Equipment

A Trimble R10 Real-Time-Kinematic (RTK) GNSS system was setup at each site location to collect accurate georeferenced data (Fig. 5). The function of this system was to provide cm level accuracy by eliminating errors present in the GPS. The Trimble R10 base station and rover receiver were utilized through the connection with the TSC3 survey controller.

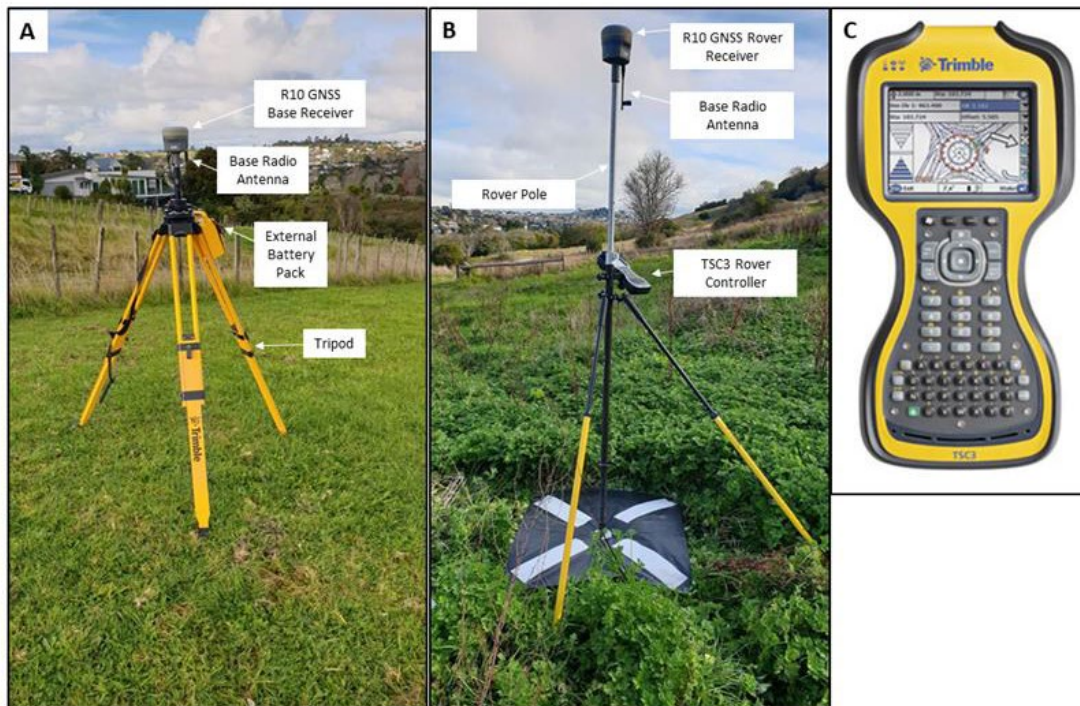


Fig. 5: A) Trimble R10 base station B) Trimble rover receiver C) Trimble TSC3 survey controller at the Orakei Landslide sites.

4.2 UAV System and Image Acquisition

UAV-derived imagery was captured by Inspire 1 and Matrice 210 RTK UAVs. On-board camera systems used for the Inspire 1 and the Matrice 210 RTK drones were the Zenmuse X3 FC350 and Zenmuse X5S FC6520 cameras, respectively (Table 4,5).

Table 4: Hardware specifications for drone models used for this study.

Model	DJI Inspire 1	DJI Matrice 210 RTK
Weight	3060g	4420g
Dimensions	437×302×453 mm	887×880×408 mm
Motor Model	DJI3510H	DJI3515
GPS Hovering Accuracy	Vertical ± (0.5 m) Horizontal ± (2.5 m)	Vertical ± (0.1 m) with RTK enabled Horizontal ± (0.1 m) with RTK enabled
Maximum Flight Time	18 min	32 min (With TB55)
Maximum Speed	79 (kph)	82.8 (kph)
Maximum Ascent Speed	5 m/s	5 m/s
Maximum Descent Speed	4 m/s	3 m/s
Max Take-off Weight	3.5 kg	6.14 kg

These cameras were attached to 360o degree rotating camera mount gimbals present at the base of the drones. This allowed for the consistent and stable collection of nadir orientated aerial imagery. Obtained imagery from each landslide location had a resolution range between 1.0 cm/px to 2.3 cm/px.

Table 5: Key camera parameters of the Zenmuse X3 FC350 and X5S FC6520 models used for the aerial UAV surveys.

Model	Zenmuse X3 FC350	Zenmuse X5S FC6520
Effective megapixels	12.76MP	20.8MP
Image Dimensions	4000×3000	5280×3956
Focal Length (mm)	4 mm	15 mm
ISO Speed	100	100
Max Aperture	1	1.53
F-stop	f/2.8	f/5

For the production of high-resolution models, a general survey is recommended a minimum 75% overlap and 60% side-overlap (Pix4D, 2019). Surveyed sites for this study attained optimal coverage with an approximate 70-80% of front overlap and 65-75% of side-overlap (e.g. Fig. 6). Surveyed flights complied with the Part 101 regulations of the Civil Aviation Authority (CAA) of New Zealand, and captured aerial imagery within the <120 m ceiling, above ground level (AGL).



Fig. 6: Example of survey flight pathways (at Orakei). A) and B) Kapa Road, C) Kawakawa Bay and D) Orere Point. Green line = flight pathway, Red dots = Image positioning.

For survey control, a minimum of five ground control points (GCPs) were distributed across each landslide site prior to each survey. The GCPs were a combination of 1 m × 1 m plastic cross mats and small wooden checkboards, and were visibility present in the acquired UAV imagery. Each GCP centre would be surveyed with the Trimble rover receiver and controller. An example of GCP distribution is shown for Orakei in Fig. 7.

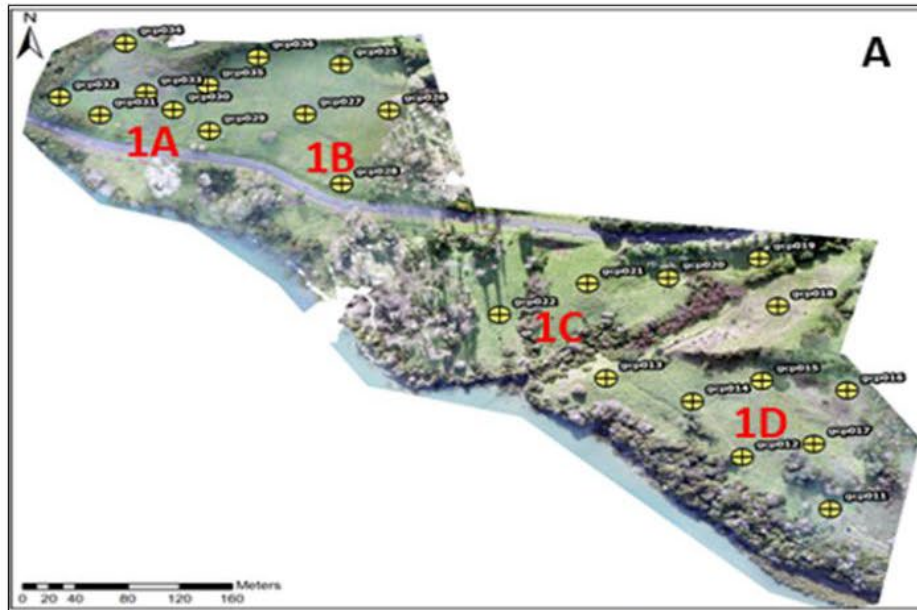


Fig. 7: Example distribution of GCPs implemented across Orakei area. Yellow circle cross = GCP.

4.3 Structure-from-Motion 3D Modelling

Structure-from-Motion photogrammetry process was implemented using the Pix4DMapper Pro 4.1.5 software. The workflow using the UAV-SfM approach for 3D modelling (Lucieer et al., 2014) followed three main phases of processing, post the flight survey acquisition and GCP distribution. These included: “Initial Processing”, “Point Cloud and Mesh generation”, and “DSM, Orthomosaic and Index generation”. An outline of the general workflow followed in this study is illustrated in Fig. 8.

SfM uses algorithms to identify matching features in a series of overlapping digital images and calculates camera location and orientation from the differential positions of multiple matched features. From these calculations, overlapping imagery is then used to reconstruct a “sparse” or “coarse” 3D point cloud model of the photographed object or surface or scene. This 3D model from the SfM method is refined to a finer resolution using Multi-View Stereopsis (MVS) methods, thereby completing the full SfM-MVS workflow (Carrivick et al., 2016). First, each image was individually inspected for image quality where blurry images were removed from the dataset.

Camera positions were loaded from the photo exchangeable image file data and calibrated with camera parameters during an “alignment” process. The camera alignment process matches points between overlapping imagery and estimates the camera positions for each photo to construct a sparse point-cloud model. Accurate GPC positioning and orientation is important (Fig. 9). The point cloud classification tool was used in Pix4D, which then allowed digital terrain models (DTMs) to be developed. In Pix4D, DTMs are

smoothed versions of the DSM, which is aimed at minimizing the effects of vegetation on the surface model.

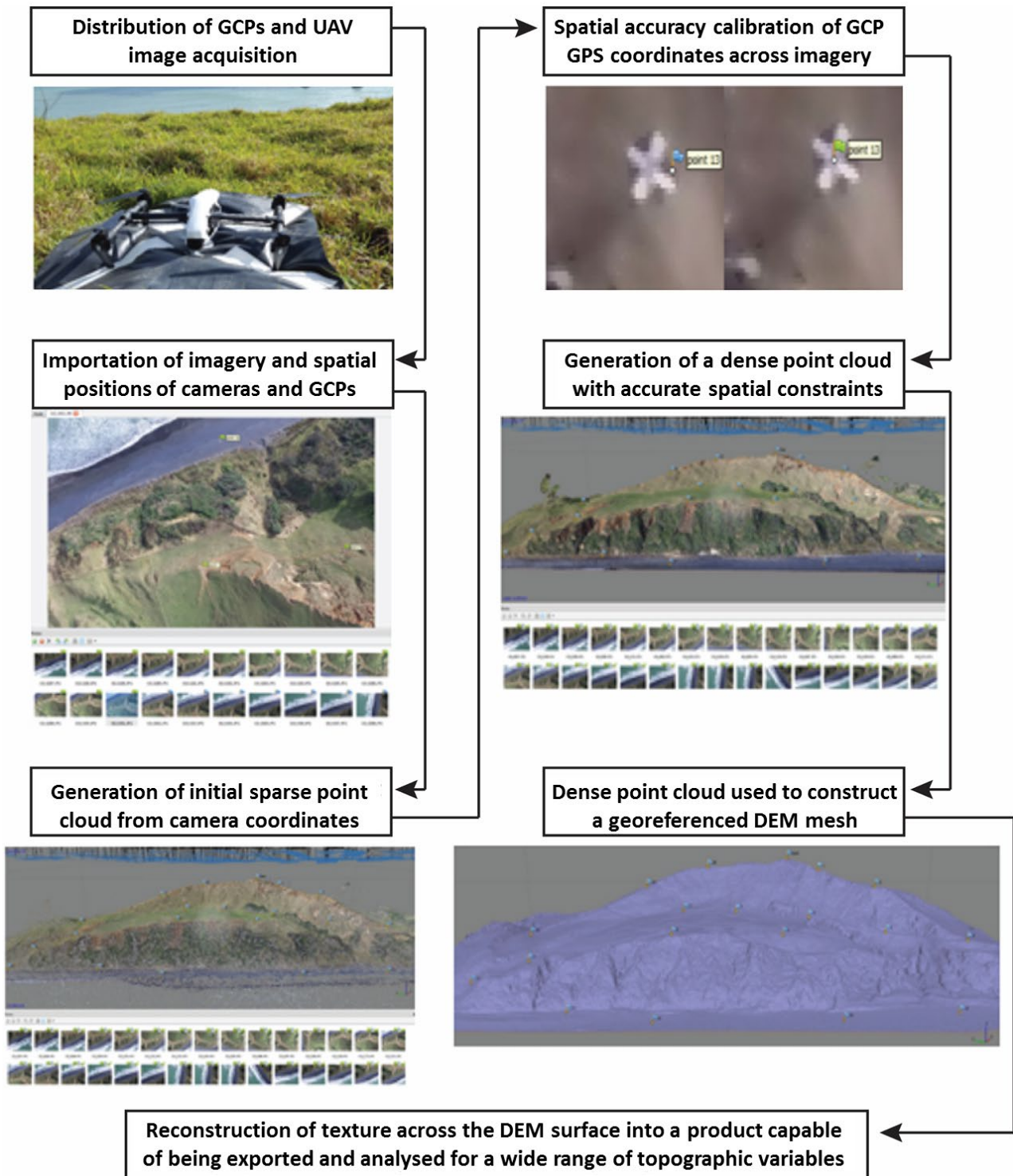


Fig. 8: SfM processing approach using Pix4D Mapper.

Accuracy and quality assessment of generated UAV-SfM models were determined through analysing resulting quality reports and error estimations for each survey site location modelled in Pix4D. Quality reports for all surveys were utilized to evaluate five major parameters for model quality. These included: (1) keypoint image matches, (2) dataset Image calibration, (3) camera optimisation, (4) calibrated Image matches, and (5) Image georeferencing. The final analytical step was DEM-differencing, for topographic

change detection using raster calculator in ArcMap 10.3. From this, DSM difference maps were calculated, by comparing the UAV-SfM data with existing LiDAR datasets.

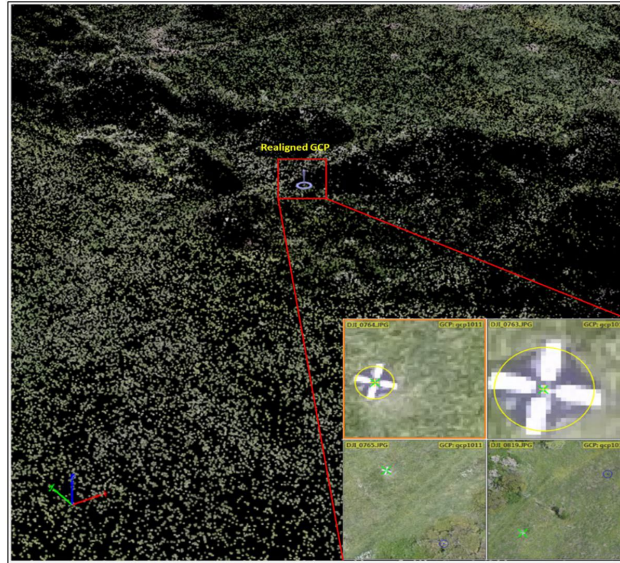


Fig. 9: Example of manual realignment procedure for imported GCPs (Orakei). Blue circle = Estimated GCP position, yellow circle = newly selected position, green cross = Reprojected 3D point and position.

4.4 Landslide change detection

Surface change detection was also trialed using COSI-Corr (Co-registration of Optically Sensed Images and Correlation), at two landslide site locations (e.g. Turner et al., 2015). Sites selected for trialling the COSI-Corr technique included 2B at Kawakawa Bay and 3A at Orere Point (Fig. 10). Both had prominent scarp features present which was ideal for where the method could be applied. For feature tracking, two pairs of DSMs at both sites for July and November of 2019 were chosen. DSMs, along with an applied hill shade effect aims to be more efficient for the COSI-Corr method than other input images like photomosaics according to Lucieer et al. (2014). Larger changes would be better identified on these DSMs with associating illumination, vegetation and surface structure changes (Turner et al., 2015). Additional 2D horizontal displacement measurements with north/south and east/west facing directional vector fields would also be generated through the implementation of this method.

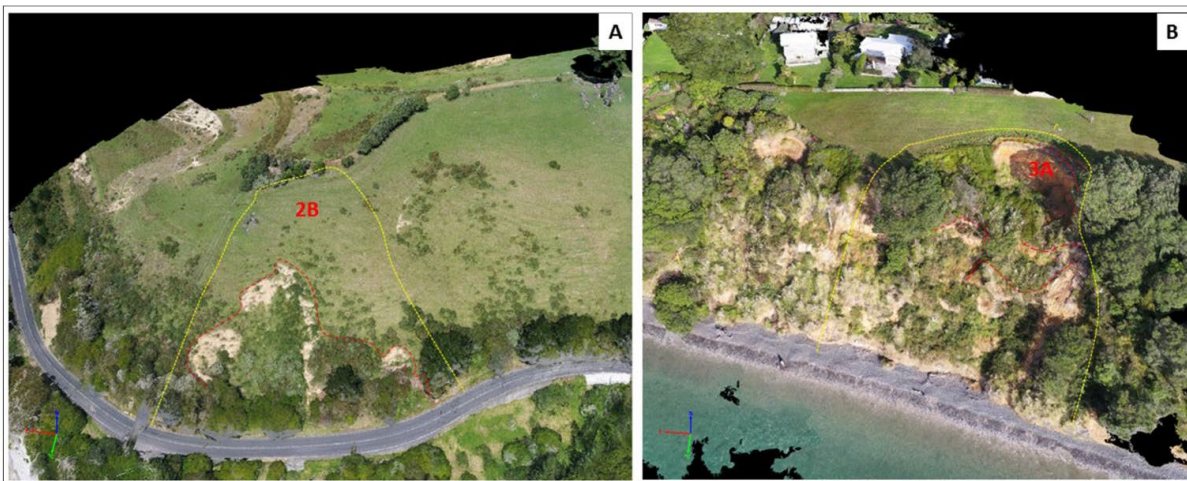


Fig. 10: Sections of interest for the COSI-Corr method for A) Kawakawa Bay 2B and B) 3B at Orere Point. Yellow line = site outline, Red line = sections of interest.

5. Results and Discussion

This section is split into structure-from motion (SfM) modelling (5.1), and DEM-differencing (5.2), and finally COSI-CORR surface change detection (5.3).

5.1 SfM modelling

5.1.1 Orakei

Sites 1A-1D at Kepa Road covered a survey area between 0.264 and 0.276 km² for July and November 2019, respectively (Table 6). For Kepa Road sites 1A-1D, models generated from the five-month interval surveys resulted in resolutions of 3.23 and 3.27 cm, respectively for both photomosaics and DSMs (Fig. 11-16). The resulting DTMs appeared at 5 × the resolution of the photomosaics and DSMs. Site 1E-1F Pix4D processing quality is shown in Table 7. The photomosaics and DSMs produced resolutions of 4.00 cm and 3.83 cm, respectively (Fig. 11-16), with a DTM resolution of 5 × 4.00 and 3.83, respectively.

With regard to the resolutions generated in the Kepa Road site models, high levels of detail of surface geomorphological features are evident. Creep is evident in limited areas within sites 1A and 1B, suggesting surface deformation. Indeed, the eastern slope flank of 1C also presents evidence of creep, however, minimal evidence of further movement is apparent during the five-month interval.

Table 6: Pix4D quality processing summary of Kepa Road sites 1A-1D.

Kepa Road, Orakei Processing Quality Summary (Sites 1A-1D)		
Parameters	July	November
<i>Area Covered</i>	0.264 km ²	0.276 Km ²
<i>Images (median keypoints per Image)</i>	53238	40412
<i>Matching (median per calibrated Image)</i>	24057.2	12512.5
<i>Average GSD (cm)</i>	3.23 cm	3.27 cm
<i>Average Point Cloud Density (Point/m³)</i>	110.4	86.5

Table 7: Pix4D quality processing summary of Kepa Road sites 1E-1F.

Kepa Road, Orakei Processing Quality Summary (Sites 1E-1F)		
Parameters	July	November
<i>Area Covered (km²)</i>	0.232	0.250
<i>Images (median keypoints per Image)</i>	54273	39922
<i>Matching (median per calibrated Image)</i>	28210.6	9389.97
<i>Average GSD (cm)</i>	4.00	3.83
<i>Average Point Cloud Density (Point/m³)</i>	74.03	98.32

Although surface deformation was minimal across each site, changes in surface vegetation was apparent for all sites. This is evident with growth in areas across sites 1A-1C, and the diminishing of vegetation particularly throughout sites 1E -1F.

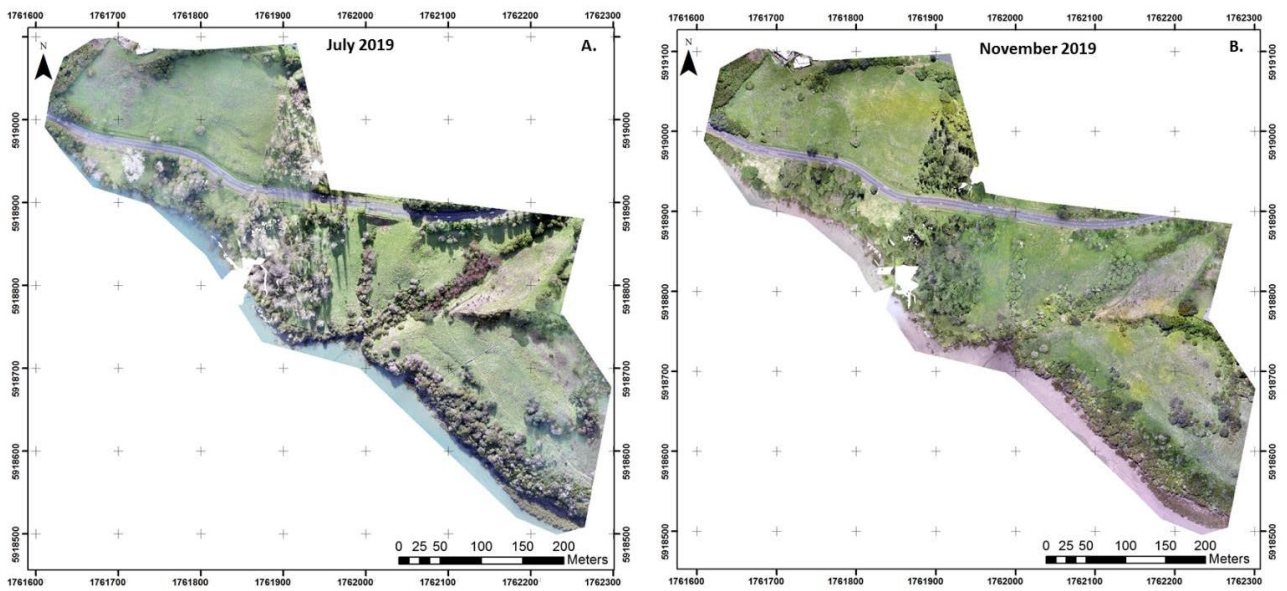


Fig. 11: Photomosaic of Kapa Road sites 1A-1D. A) Left = July 2019, B) Right = November 2019.

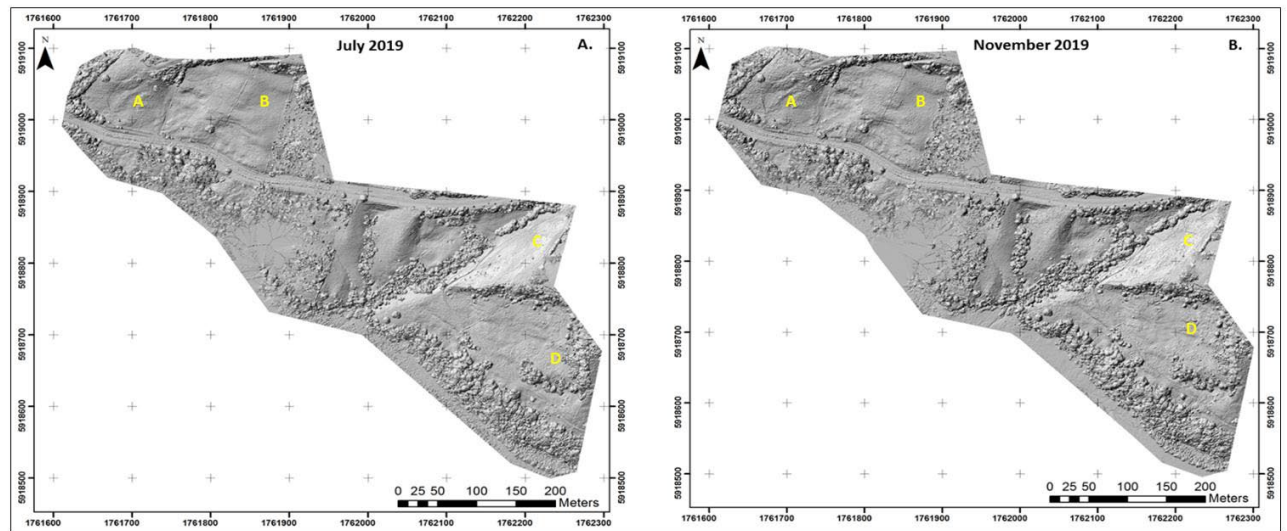


Fig. 12: Hillshade DSMs of Kapa Road sites 1A-1D. A) Left = July 2019, B) Right = November 2019.

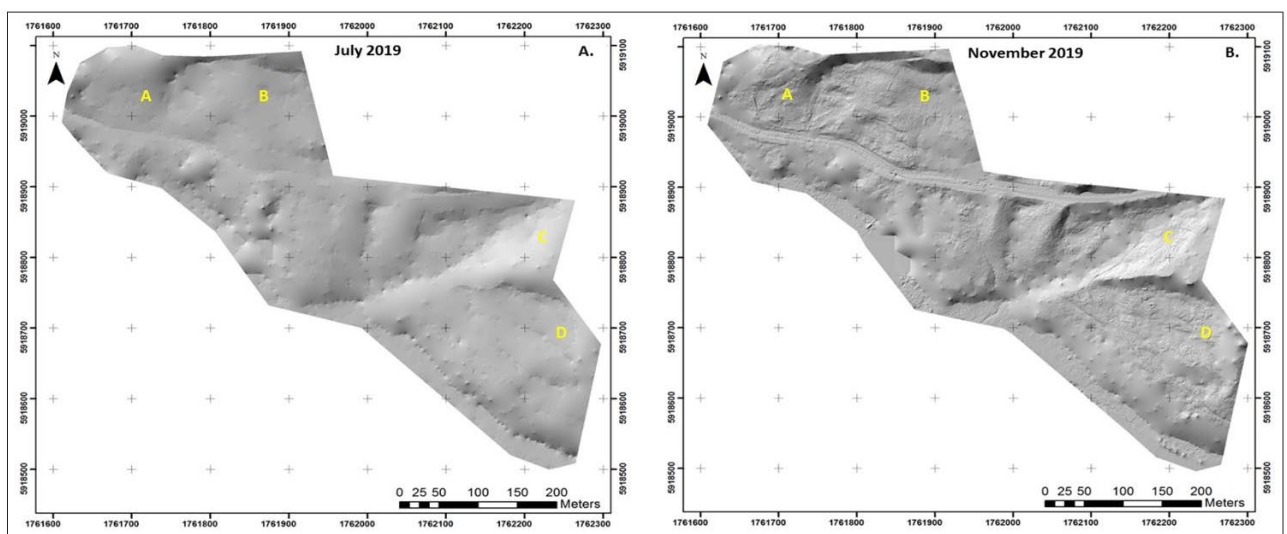


Fig. 13: Hillshade DTMs of Kapa Road sites 1A-1D. A) Left = July 2019, B) Right = November 2019.

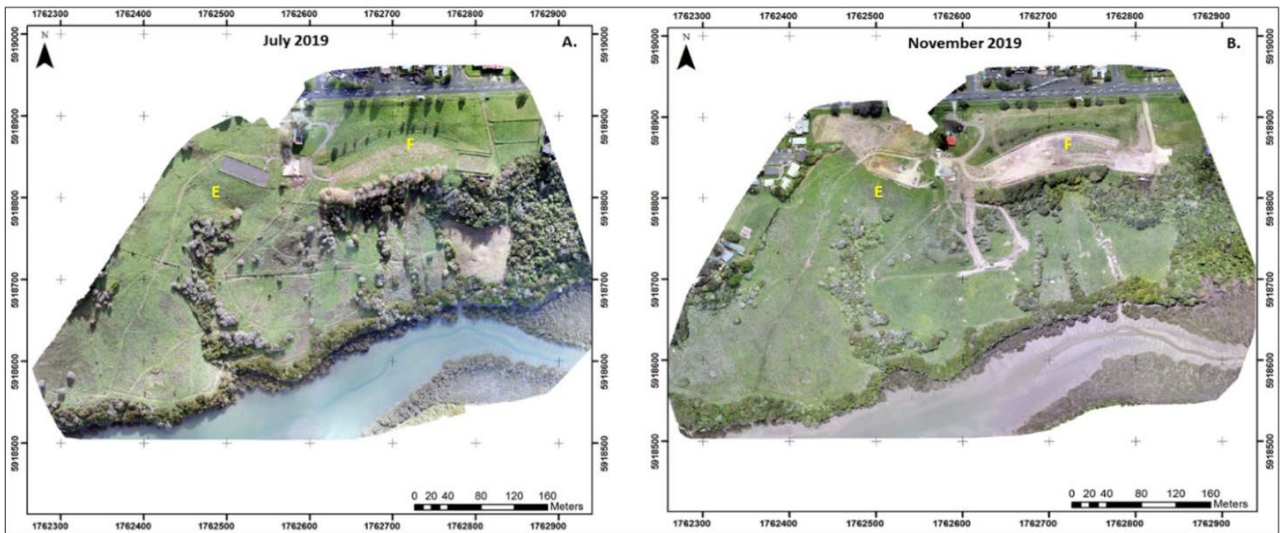


Fig. 14: Photomosaic of Kapa Road sites 1E–1F. A) Left = July 2019, B) Right = November 2019.

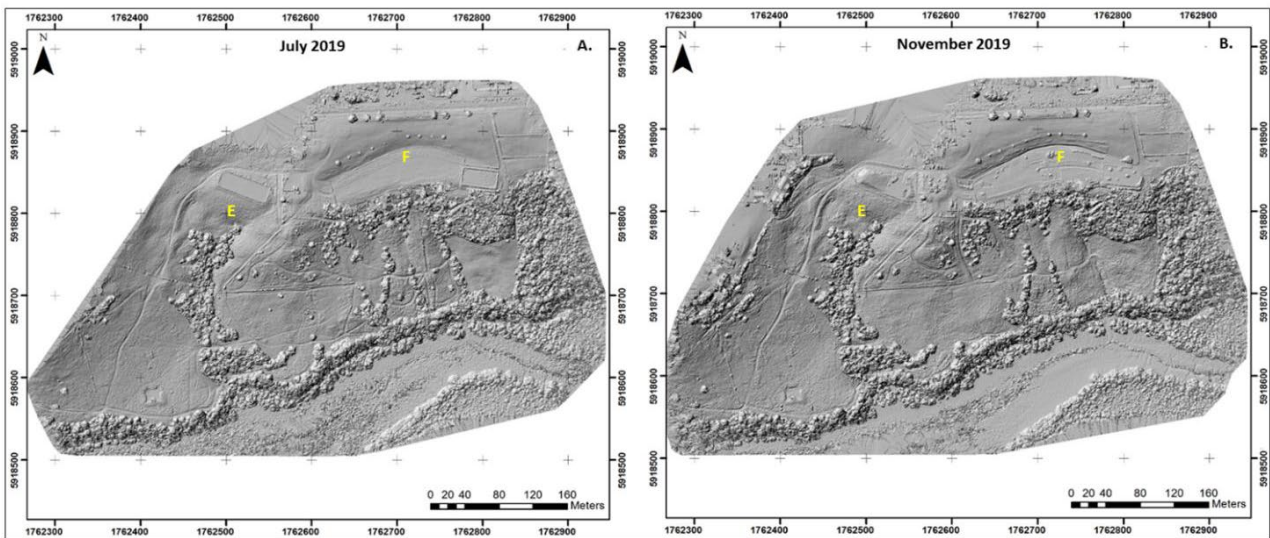


Fig. 15: Hillshade DSMs of Kapa Road site 1E –1F. A) Left = July 2019, B) Right = November 2019.

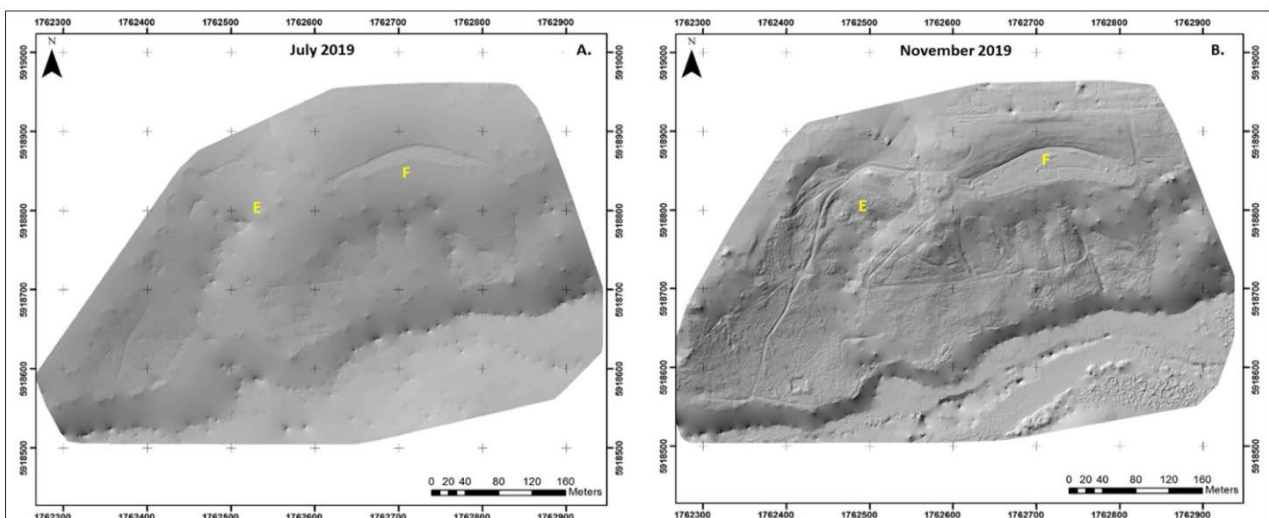


Fig. 16: Hillshade DTMs of Kapa Road site 1E -1F. A) Left = July 2019, B) Right = November 2019.

5.1.2 Kawakawa Bay

Between sites 2A and 2B at Kawakawa Bay, the surveying area covered between 0.083 and 0.118 km² (Table 8). The processed ground sampling distance (GSD) across sites 2A and 2B was similar between the two surveys, averaging 2.09 and 2.13 cm, respectively.

Table 8: Pix4D quality processing summary of Kawakawa Bay sites 2A-2B.

Kawakawa Bay Processing Quality Summary (Sites 2A-2B)		
Parameters	July	November
Area Covered (km ²)	0.083	0.118
Images (median keypoints per Image)	70525	62409
Matching (median per calibrated Image)	36980.1	19484.4
Average GSD (cm)	2.09	2.13
Average Point Cloud Density (Point/m ³)	376.46	193.91

Generated photomosaic and DSMs for Kawakawa Bay sites 2A-2B were of 2.09 and 2.13 cm resolution respectively (Fig. 17-19). The associating DTM resolutions for sites 2A and 2B were 5 × 2.09 and 2.13, respectively (Fig. 19). Photomosaics generated for Kawakawa Bay produced resolutions of c. 2 cm (Fig. 17).

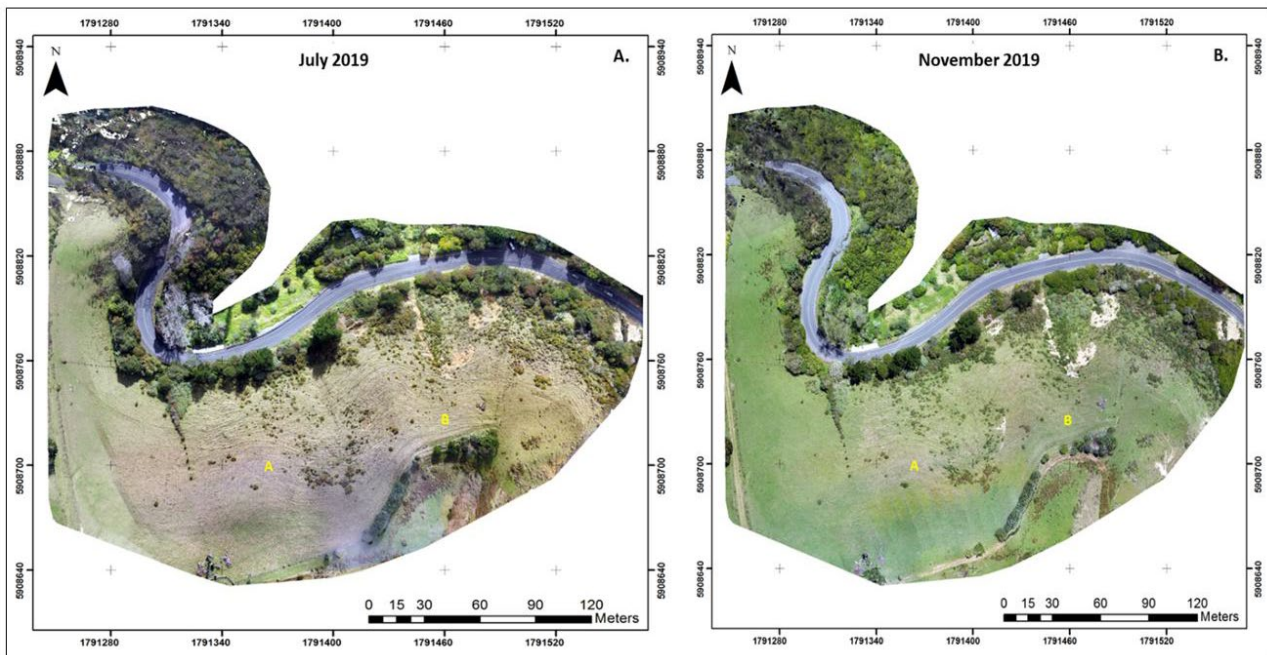


Fig. 17: Photomosaic of Kawakawa Bay sites 2A – 2B. A) Left = July 2019, B) Right = November 2019.

As dense vegetation coverage was removed across sites 2A and 2B in the DTMs, particularly across the toe regions, it was difficult to detect slope deformation across the five-month interval. Changes detected across the Kawakawa Bay sites appear limited to surface vegetation.

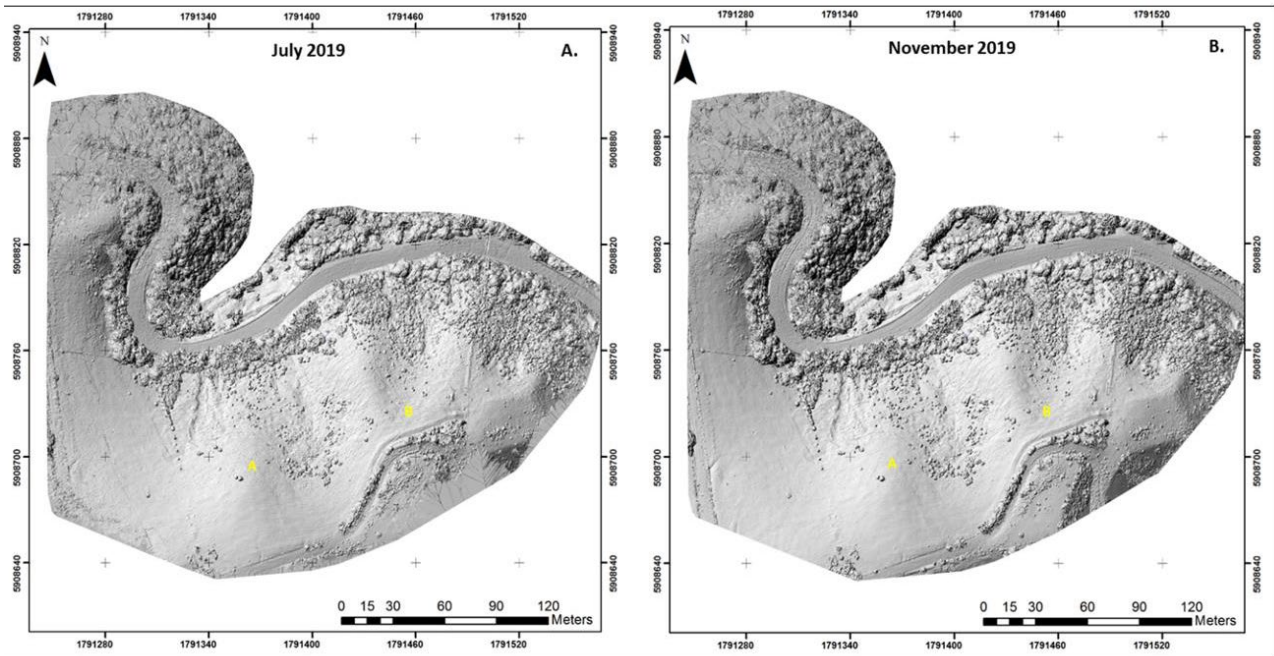


Fig. 18: Hillshade DSMs of Kawakawa Bay sites 2A – 2B. A) Left = July 2019, B) Right = November 2019.

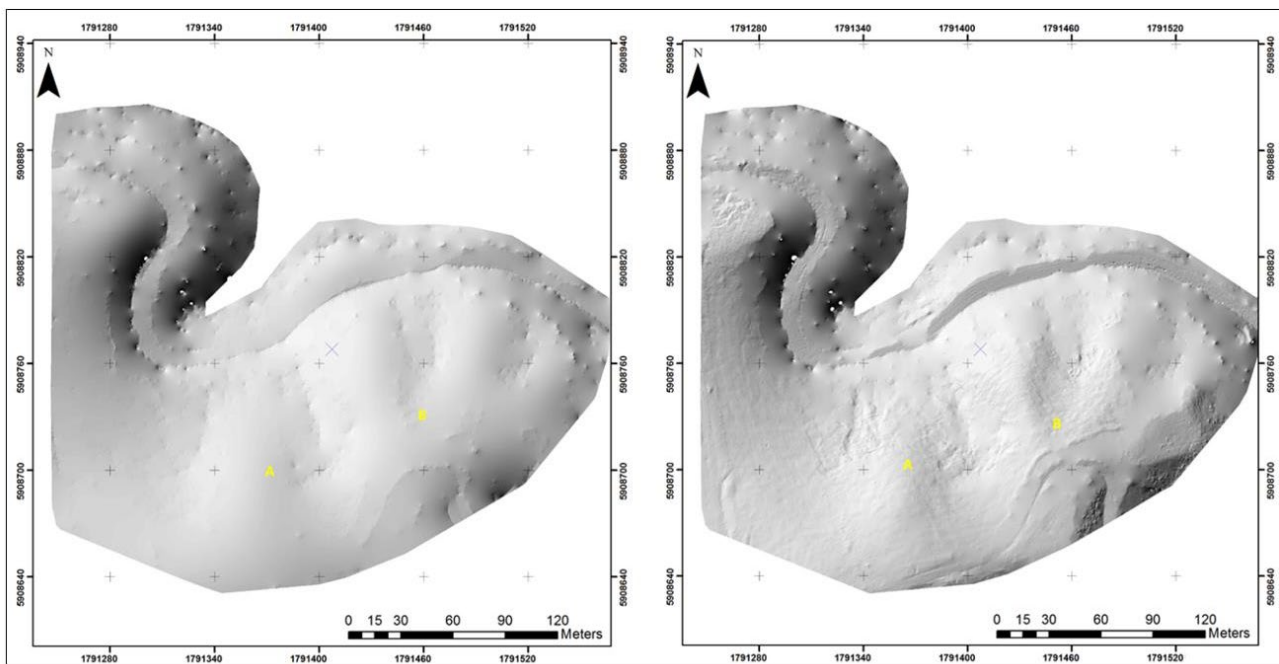


Fig. 19: Hillshade DTMs of Kawakawa Bay sites 2A – 2B. A) Left = July 2019, B) Right = November 2019.

5.1.3 Orere Point

These are the smallest sites in this research project, with the surveying area covering 0.017 in July and 0.022 km² in November. The average generated GSD recorded for sites 3A and 3B were 1.72 and 1.80 cm, respectively (Table 9). Surface vegetation change is likely the cause of c. 122.08 point/m³ difference between July and November. Photomosaics and DSMs had the same 1.72 and 1.80 cm model resolution (Fig. 20-22). As with previous DTMs for July and November, model resolution was generated at 5 × that of

the photomosaic and DSM. Photomosaic resolutions were <2 cm for both July and November, although vegetation coverage is apparent across both sites 3A and 3B. Nevertheless, the headscarps at both 3A and 3B are dominant features highlighted on both the photomosaic and DSMs.

Table 9: Pix4D quality processing summary of Oরে Point sites 3A-3B.

Oরে Point Processing Quality Summary (Sites 3A-3B)		
Parameters	July	November
Area Covered (km ²)	0.017	0.022
Images (median keypoints per Image)	69415	63440
Matching (median per calibrated Image)	17179.9	13037.1
Average GSD (cm)	1.72	1.80
Average Point Cloud Density (Point/m ³)	716.86	594.78

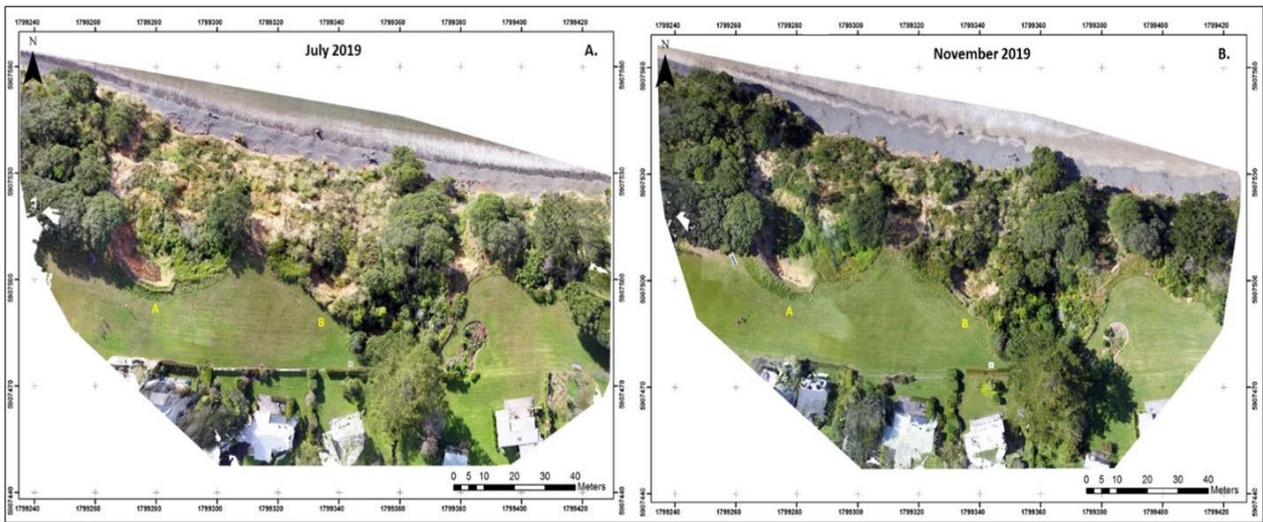


Fig. 20: Photomosaic of Oরে Point sites 3A – 3B. A) Left = July 2019, B) Right = November 2019.

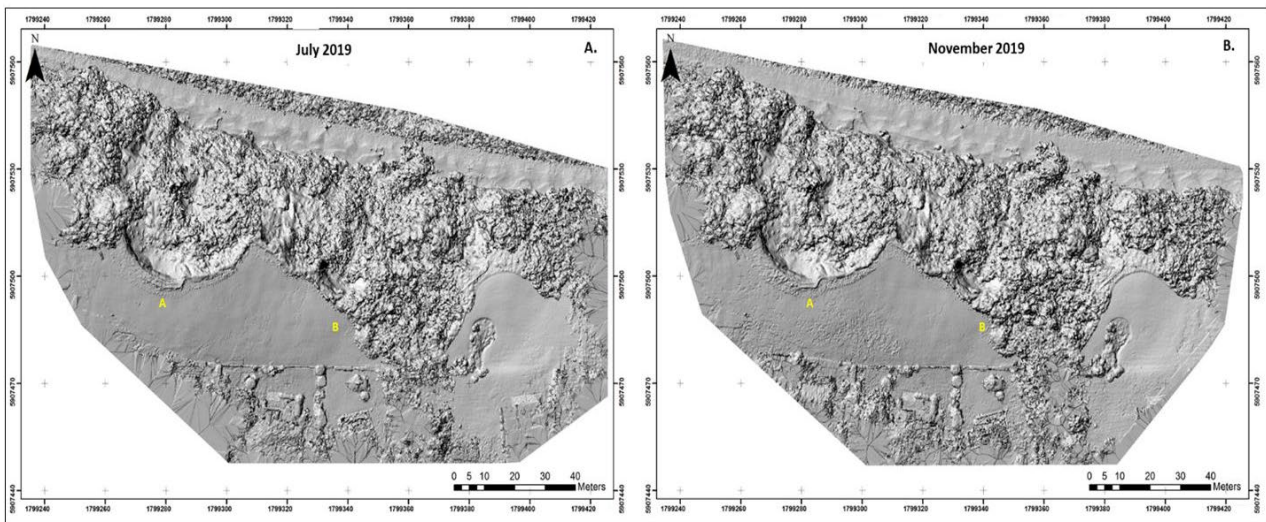


Fig. 21: Hillshade DSMs of Oরে Point sites 3A – 3B. A) Left = July 2019, B) Right = November 2019.

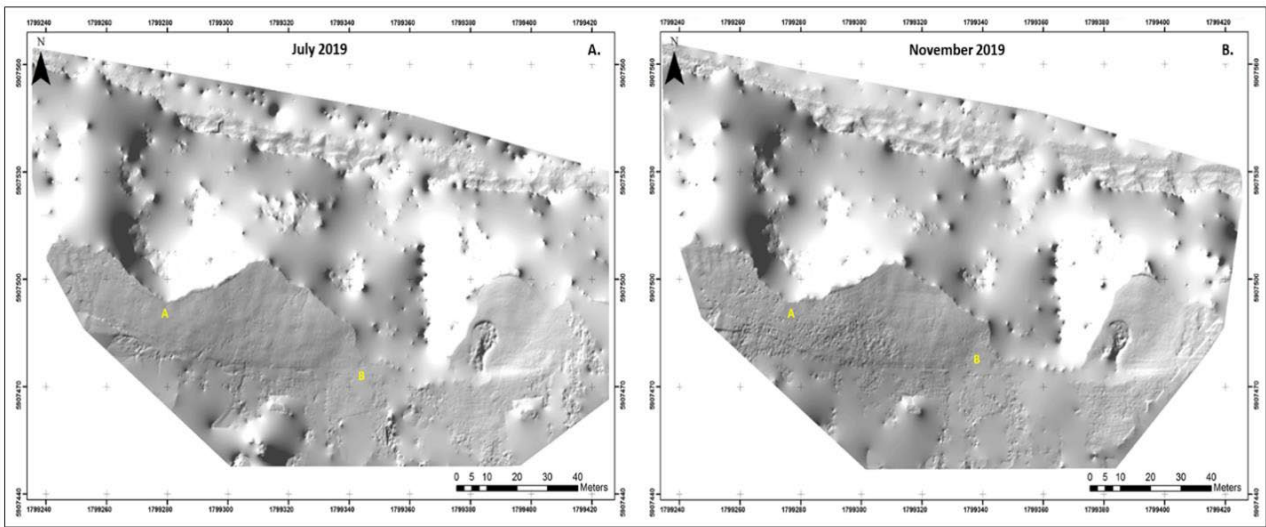


Fig. 22: Hillshade DTMs of Orere Point sites 3A – 3B. A) Left = July 2019, B) Right = November 2019.

5.2 DEM of Differencing (DEMoD) Analysis

Differencing of UAV-SfM generated DSMs of July 2019, was undertaken via comparison with the c. 1 m resolution 2016 LiDAR DEM dataset of Auckland (available via LINZ). DSM-differencing models are presented in this section illustrating the surface deformation occurring between 2016 and 2019. Differencing of a five-month survey interval is then be presented between July and November of 2019.

5.2.1 Orakei

Analysing the generated DSMoD for Kepa Road sites 1A-1D, the total deformation defined was between +28.83 m and -1.32 m across the wider site between 2016-2019 (Fig. 23). However, the high of + 28.83 m is likely to be an artefact of the tall tree vegetation present along the lower slope regions of sites 1A-1B. Real, non-artefact surface movement due to creep and deformation was visible around gully heads, but was minimal with a range between -0.010 m and -0.056 m.

A five-month survey interval (July-November 2019) DSMoD was generated for comparison with the three year multi-temporal period. Visual deformation was minimal across the slope faces, for sites 1A-1D (Fig. 24). The DSMoD of sites 1E-1F across the 2016-2019 period produced deformation between +14.71 m and -2.86 m (Fig. 25). When evaluating the generated site 1E-1F DSMoD for the five-month interval, no differences indicative of surface deformation were visible (Fig. 26). Rather, any changes are probably due to earthworks.

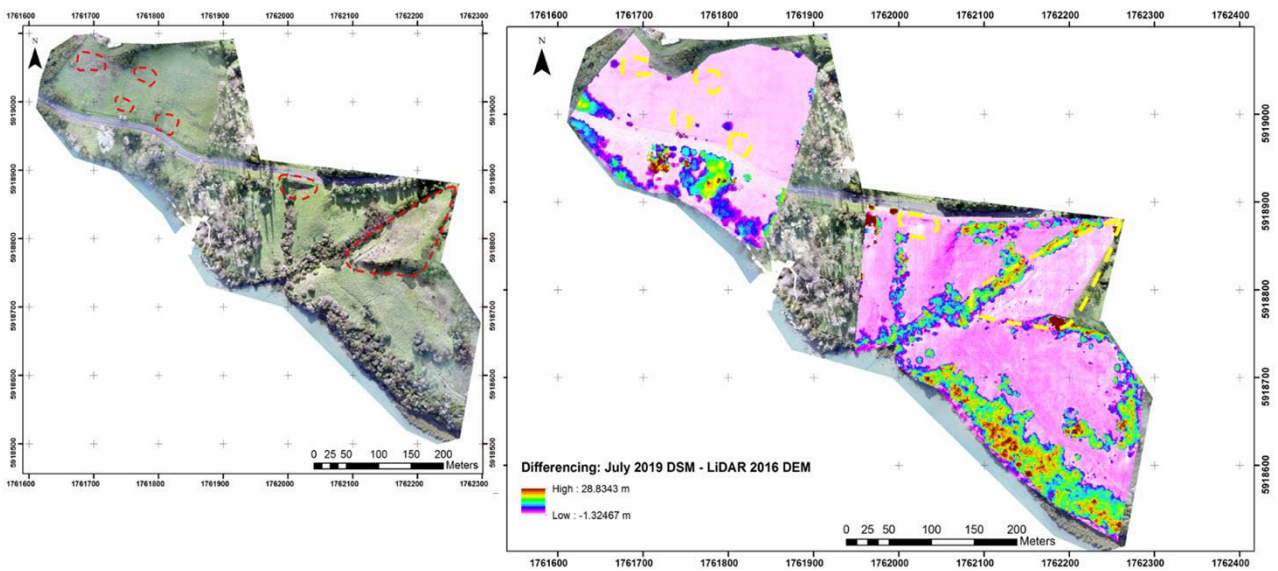


Fig. 23: DSM-differencing model of Kepa Road sites 1A-1D from UAV-SfM derived July 2019 DSM and 2016 LiDAR DEM. Red boundaries on photomosaic (left), correlating with yellow boundaries (right). Boundaries illustrate regions of interest.

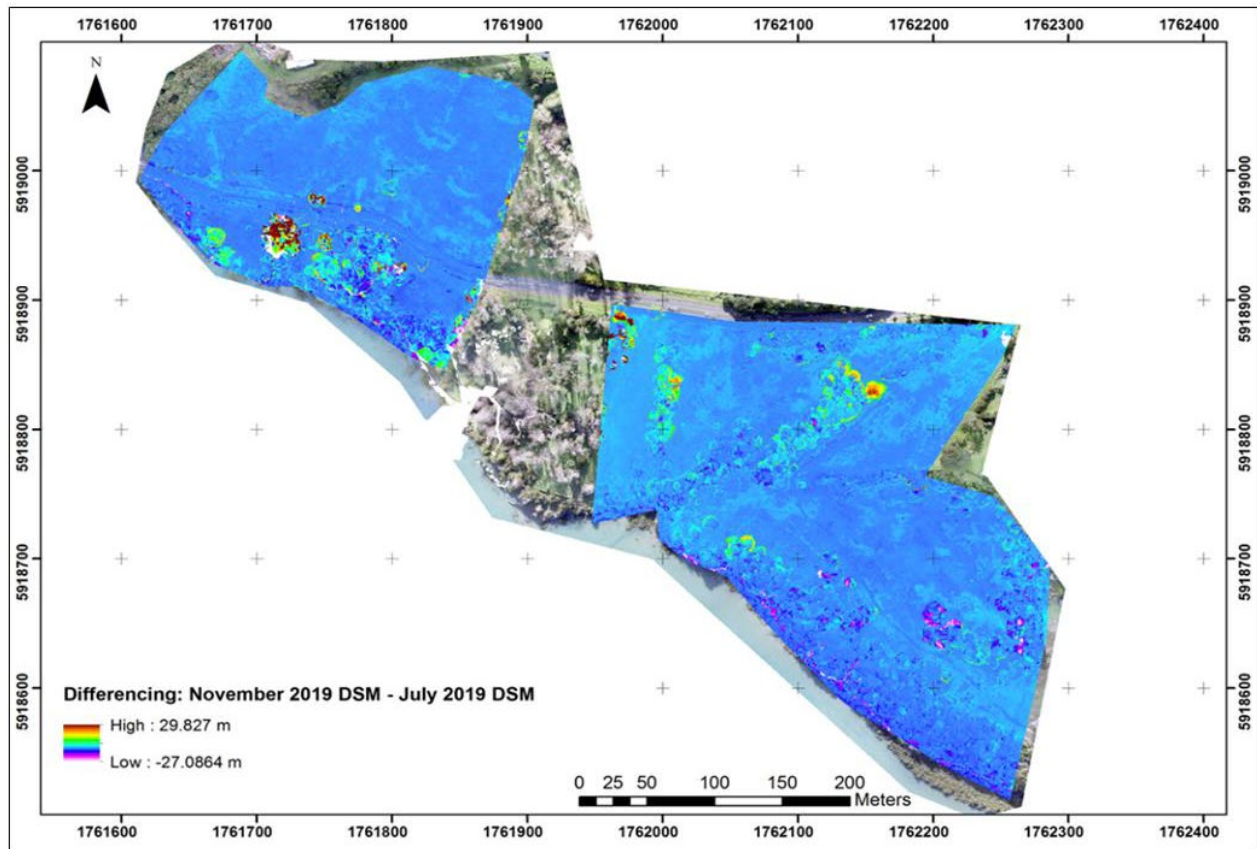


Fig. 24: DSM-Differencing model of Kepa Road sites 1A-1D. July 2019 DSM subtracted from the November 2019 DSM.

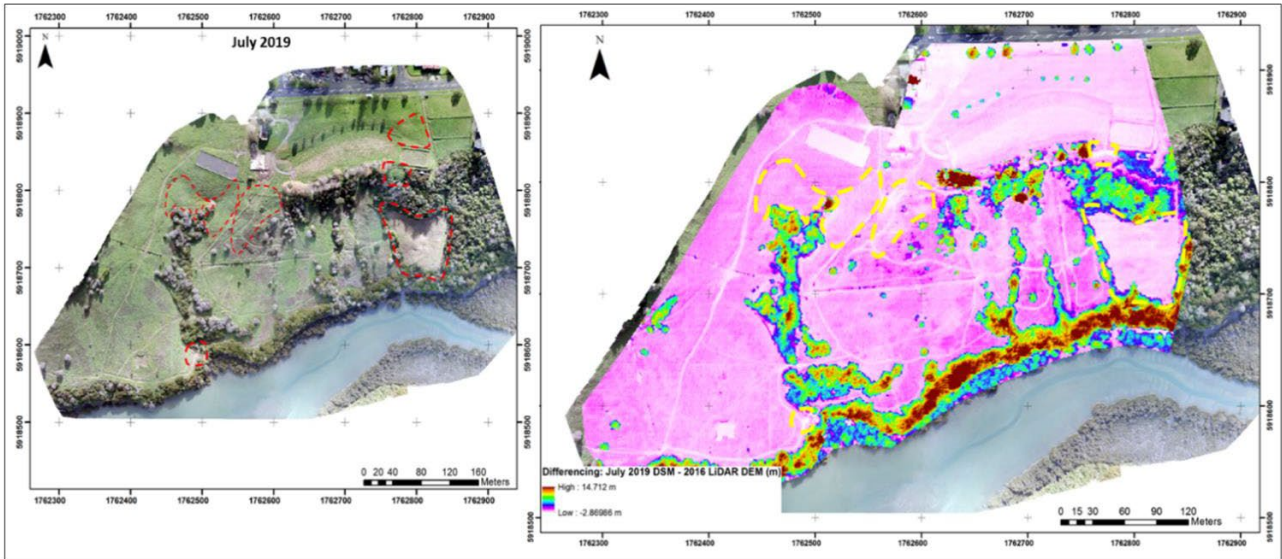


Fig. 25: DSM-differencing model of Keka Road sites 1E-1F. UAV-SfM derived July 2019 DSM and 2016 LiDAR DEM. Red boundaries on photomosaic (left), correlating with yellow boundaries (right). Boundaries illustrate regions of interest.

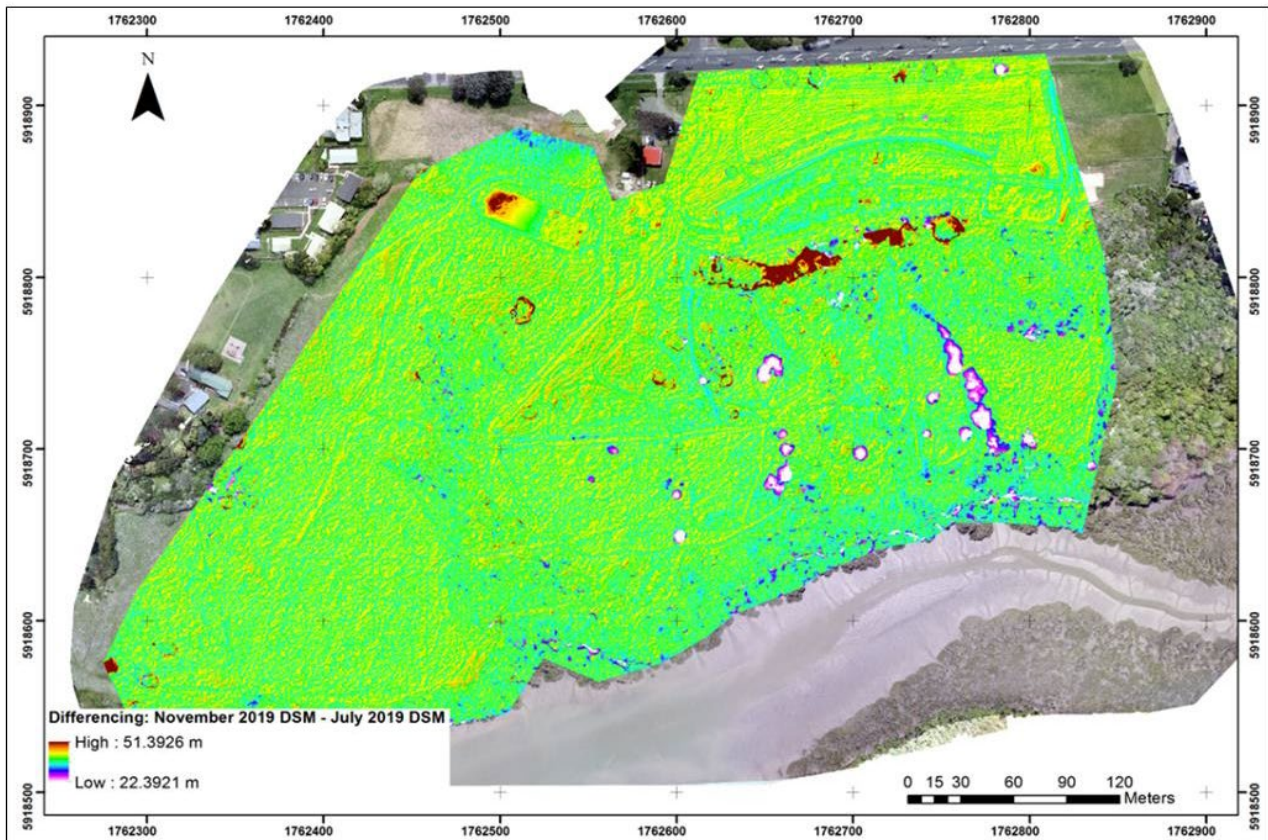


Fig. 26: DSM-Differencing model of Keka Road sites 1E-1F. July 2019 DSM subtracted from November 2019 DSM.

5.2.2 Kawakawa Bay

DSMoD models produced for sites 2A-2B at Kawakawa Bay recorded a range between +27.02 m and -2.97 m over the three-year period 2016-2019 (Figure 27, 28).

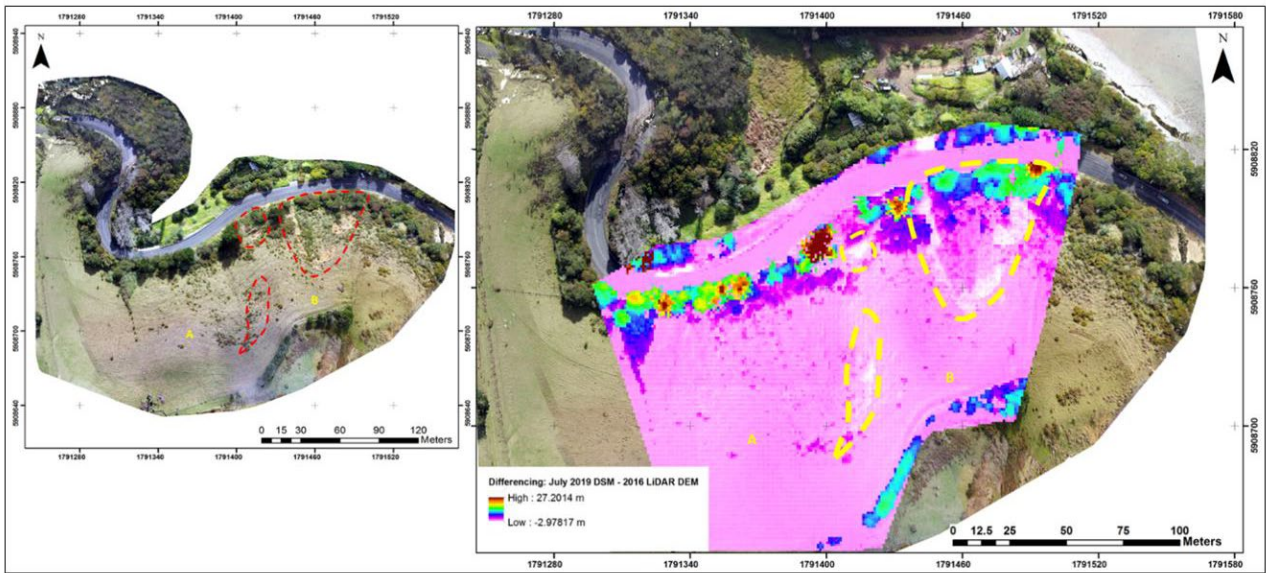


Fig. 27: DSM-differencing model of Kawakawa Bay sites 2A and 2B. UAV-SfM derived July 2019 DSM and 2016 LiDAR DEM. Red boundaries on photomosaic (left), correlating with yellow boundaries (right). Boundaries illustrate regions of interest.

The high of 27.02 m was actually an artefact of vegetation across the toe regions of sites 2A-2B. However, the loss of -2.97 m was present south of site 2B, past the Clevedon-Kawakawa Bay Road. This represents landslide activity in the form of a minor roadside slump.

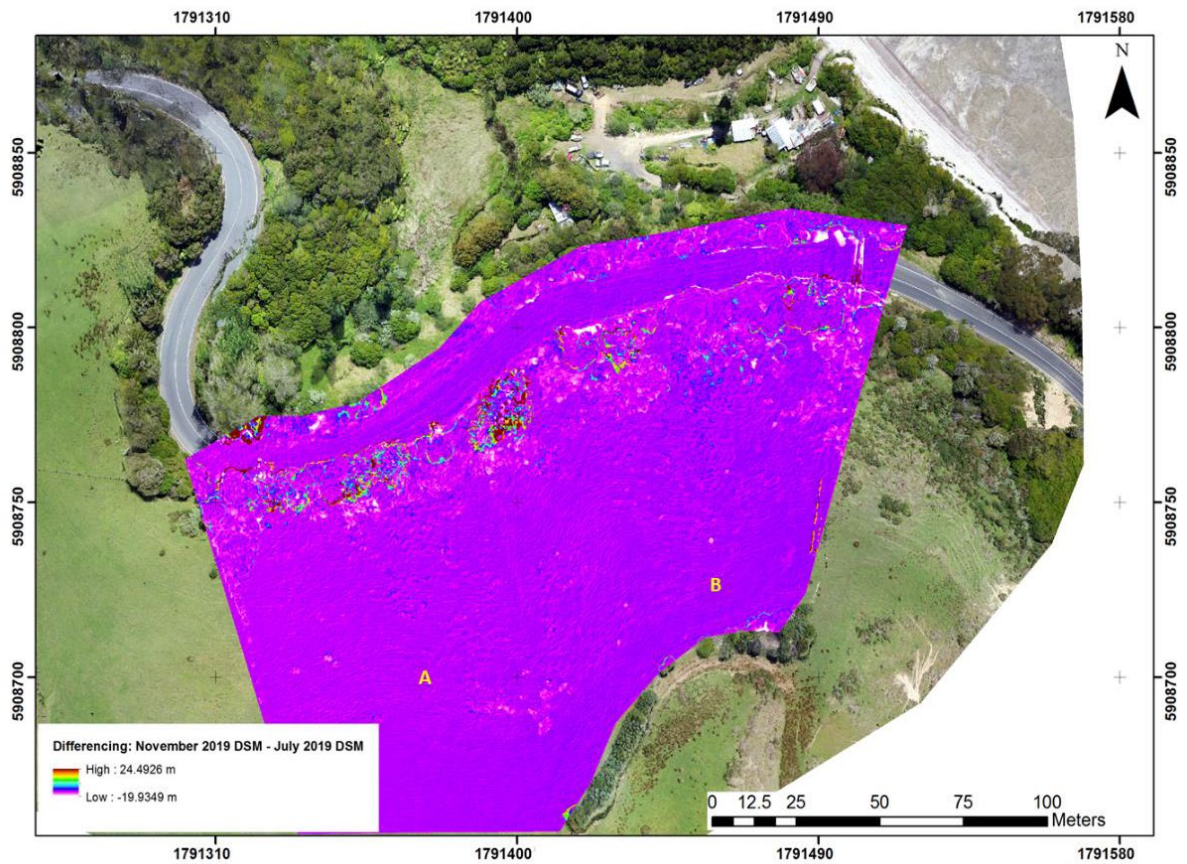


Fig. 28: DSM-Differencing model of Kawakawa Bay sites 2A and 2B. July 2019 DSM subtracted from the November 2019 DSM.

5.2.3 Orere Point

The generated DSMoD model for sites 3A-3B at Orere Point generated change of +34.31 m (mostly vegetation) and -5.84 m over 2016-2019 (Fig. 29). However, the “low” of -5.84 m indicates formation of a rounded-scarp at site 3A. Notable deformation zones are highlighted in Fig. 29. Surface loss across site 3A appears to have a range between -5.84 m and -0.0084 m. This is due to a small scarp failure at the border of site 3A-3B, and a planar slide. Site 3B shows deformation ranging from -4.7 m to -0.01 m across the slope surface as illustrated on the DSMoD, but these seem to be survey artefacts, rather than landslide activity. The generated DSMoD across the five-month interval July-November 2019, produced a range between +36.71 m and -4.48 m (Fig. 30), but this seems to be vegetation growth artefacts.

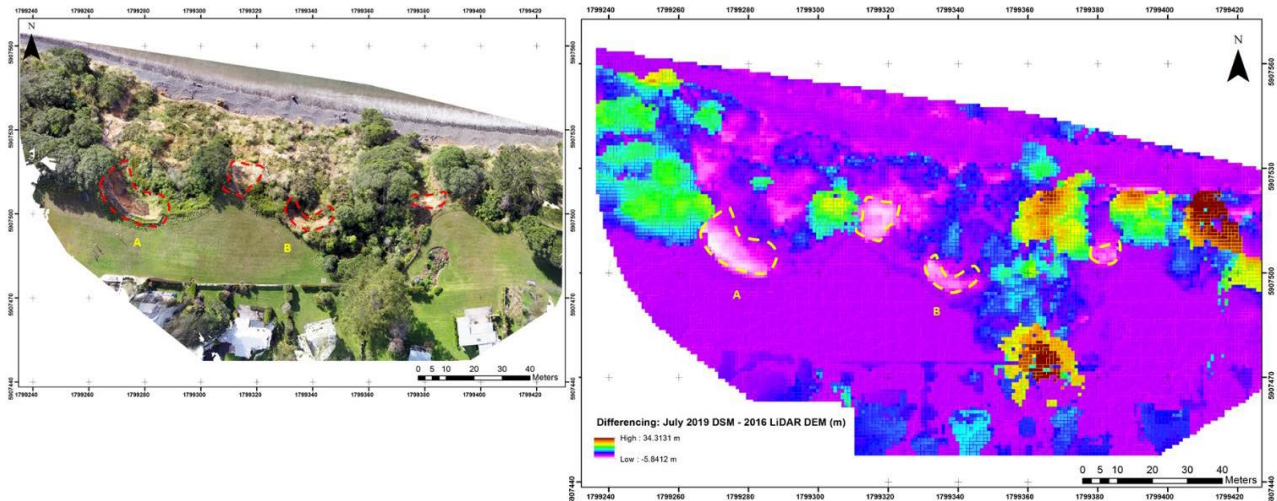


Fig. 29: DSM-differencing model of Orere Point 3A–3B. UAV-SfM derived July 2019 DSM and 2016 LiDAR DEM. Red boundaries on photomosaic (left), correlating with yellow boundaries (right). Boundaries illustrate regions of interest.

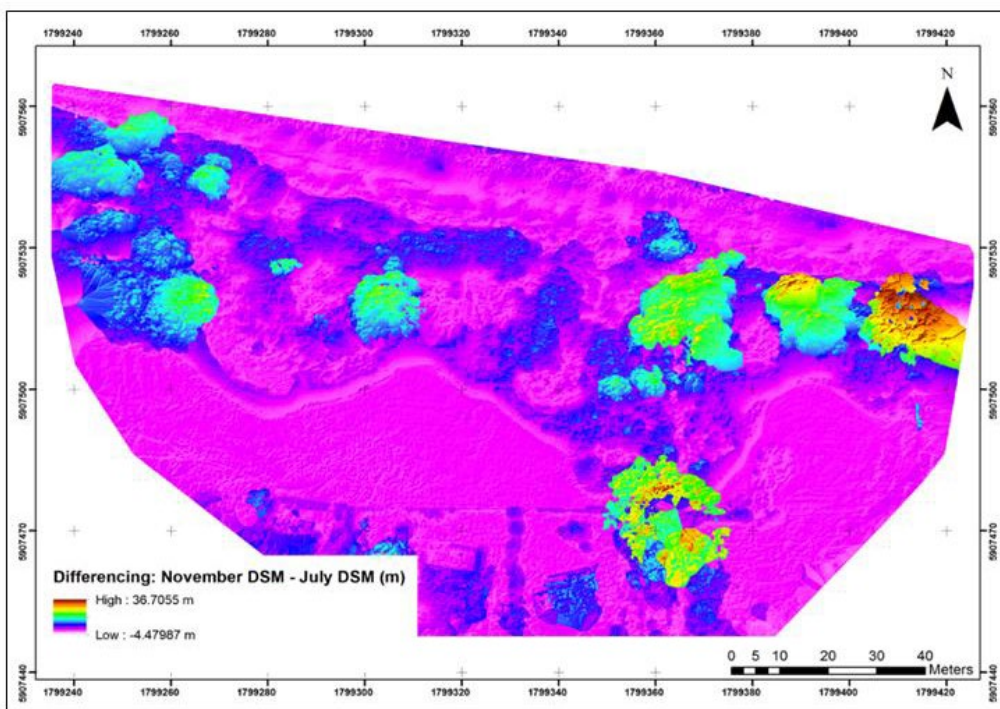


Fig. 30: DSM-Differencing model of Orere Point 3A–3B (July 2019 DSM subtracted from Nov 2019 DSM).

5.3 COSI-Corr analysis

COSI-Corr surface change analysis was limited to trials at Kawakawa bay (sites 2B) and Orere point (site 3A), as these seemed to provide scope for the method to be successful. Following Lacroix et al. (2018), a “Layer Stacking” procedure of the “Pre-event” and “Post-event” orthomosaics for sites 2B and 3A was conducted. This was followed by the final correlation of the two layers which produced displacement maps in the east/west and north/south directions along with a signal-to-noise ratio (SNR) generated map. The resultant deformation vectors and magnitudes are shown in Figures 31 and 32, respectively.

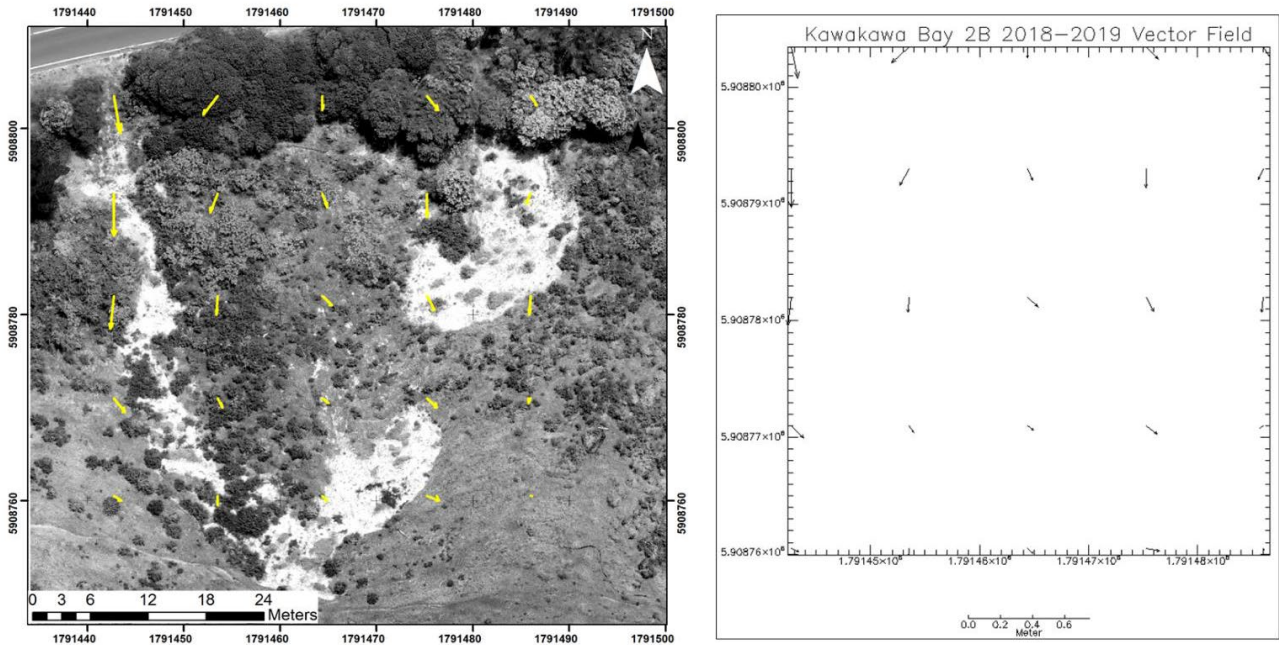


Fig. 31: Vectors overlain across site 2B (left). Associated vector field outlining displacement magnitude and direction (right).

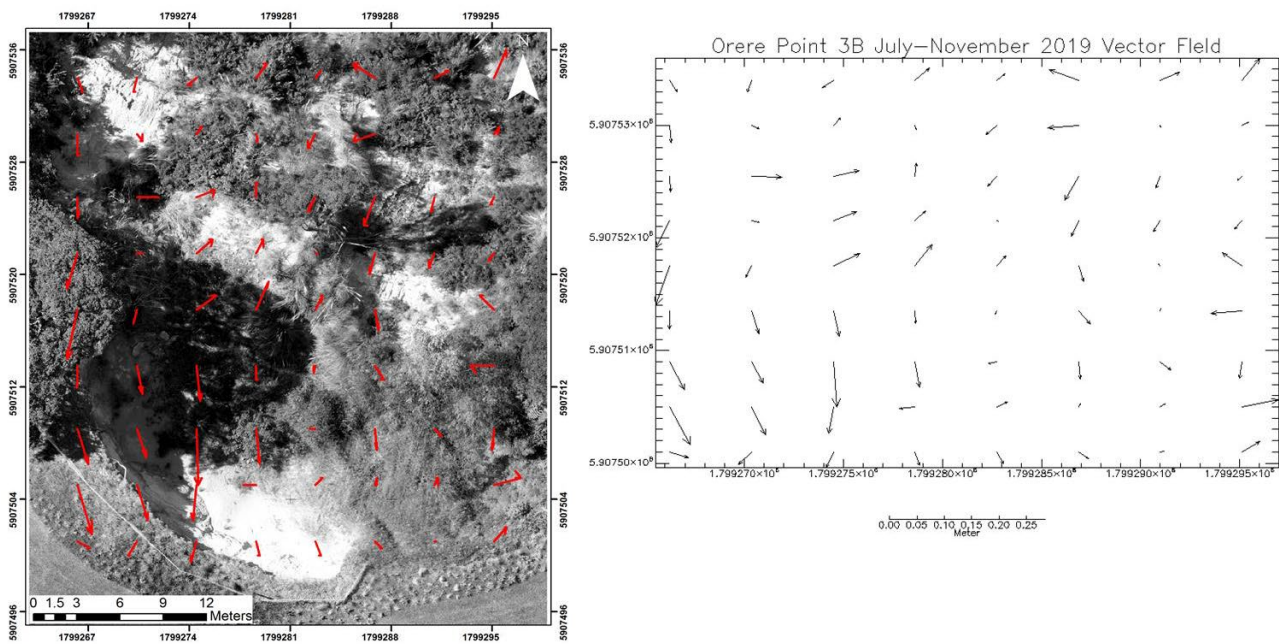


Fig. 32: Vectors overlain across site 3A (left). Associated vector field outlining displacement magnitude and direction (right).

However, vector directions do not appear to deform in the expected direction, and the geomorphological characteristics of sites 2B and 3A show clear downslope (or sometimes, cross-slope) movement. COSI-Corr appears of limited value, possibly due to a lack of time-consuming manual filtering (e.g. Ding et al., 2020).

6. Conclusions and key findings

It would appear that the studied landslides fall into the category of Class 1 and Class 2 from Varnes (1978) velocity classification. This means that in situ monitoring in the future to reduce the impact of landslide hazard on residential properties, road and infrastructure could focus on the methods outlined in Uhlemann et al. (2016) may provide the most useful deformation monitoring methods. Nevertheless, 3D aerial monitoring via UAV photogrammetry can be useful in particular locations, for ongoing monitoring, but also as part of a landslide response programme.

7. Future work

- Monitoring could continue using UAV-SfM, but longer time intervals may be more likely to generate detectable deformation.
- Without a significant failure event, the detection of subtle slope movements across a short survey interval using DEM-differencing will likely prove challenging to identify.
- If trials using the COSI-Corr feature tracking analysis technique continue, manual filtering, which can be time consuming, should be trialled using ArcMap.
- Utilization of PPK and RTK UAV systems should be considered for future slope monitoring studies. For PPK UAVs, neither GNSS base station to drone base station, nor drone base station to drone correction data communications are required; only the telemetry between drone and drone base station is needed. Both RTK and PPK negate the need for GCPs, which can be time consuming to set-out.
- Because of vegetation cover on many Auckland sites, developing accurate terrain models below vegetation useful for time series analysis via differencing can be problematic. UAV LiDAR systems, where the vegetation returns can easily be filtered may be advantageous, and the last 2-3 years has seen the rapid emergence of a wide range of off-the-shelf UAV-LiDAR systems such as RIEGL VUX-1, and the Leica ALS80 Airborne LiDAR Sensor.

Acknowledgements

In particular, Ngāti Whātua Ōrākei are thanked for allowing access at several times to their land, as well as various other landowners across the city and region.

References

- Brook MS, Merkle J. (2019). Monitoring active landslides in the Auckland region utilising UAV/structure-from-motion photogrammetry. *Japanese Geotechnical Society Special Publication* 6(2): 1-6.
- Brook MS. (2018). Field reconnaissance of the Rawene Slip urban landslide, Auckland, New Zealand. *Landslides* 15(11): 2295-2302.
- Carrivick HL, Smith WM, Quincey DJ. (2016). *Structure from Motion in the Geosciences*. Wiley-Blackwell.
- Cruden DM, Varnes DJ. (1996). Landslide types and processes. *Landslides: investigation and mitigation, Volume Special report 247*: 36-75.

- Ding C, Zhang L, Liao M, Feng G, Dong J, Ao M, Yu Y. (2020). Quantifying the spatio-temporal patterns of dune migration near Minqin Oasis in northwestern China with time series of Landsat-8 and Sentinel-2 observations. *Remote Sensing of Environment* 236: 1-24.
- Edbrooke SW. (2001). *Geology of the Auckland Area: Scale 1: 250 000*. Institute of Geological & Nuclear Sciences
- Faulkner M, Saunders G. (2008). Landslip Stabilisation - Turei Hill, Kawakawa Bay. 1-12.
- Hungr O, Leroueil S, Picarelli L. (2014). The Varnes classification of landslide types, an update. *Landslides* 11(2): 167-194.
- Lacroix P, Bièvre G, Pathier E, Kniess U, Jongmans D. (2018). Use of Sentinel-2 images for the detection of precursory motions before landslide failures. *Remote Sensing of Environment* 215: 507-516.
- Lucieer A, Jong SMD, Turner D. (2014). Mapping landslide displacements using Structure from Motion (SfM) and image correlation of multi-temporal UAV photography. *Progress in Physical Geography* 38: 97-116.
- Nemeth K, Agustin-Flores J, Briggs R, Cronin SJ, Kereszturi G, Lindsay JM, Pittari A, Smith IEM. (2012). Monogenetic volcanism of the South Auckland and Auckland Volcanic Fields. In *IAVCEI-IASIMC Conference, Auckland, New Zealand*. 1-72.
- O'Brien E. (2019). *Engineering geology of Orere Point, Auckland*. Unpublished BSc Hons dissertation, University of Auckland.
- Pix4D. (2019). How to verify that there is enough overlap between the images. Retrieved from: <https://support.pix4d.com/hc/en-us/articles/203756125-How-to-verify-that-there-is-enough-overlap-between-the-images>
- Rosser B, Dellow S, Haubrock S, Glassey P. (2017). New Zealand's national landslide database. *Landslides* 14(6): 1949-1959.
- Rotaru A, Oajdea D, Răileanu P. (2007). Analysis of the landslide movements. *International Journal of Geology* 1(3): 70-79.
- Ryder K, (2019) *A UAV photogrammetry/DFN modelling approach of analysing rockfall along Auckland's coastal cliffs*. Master's thesis, University of Auckland, Auckland, New Zealand.
- Turner D, Lucieer A, De Jong SM. (2015). Time series analysis of landslide dynamics using an unmanned aerial vehicle (UAV). *Remote Sensing* 7(2): 1736-1757.
- Uhlemann S, Smith A, Chambers J, Dixon N, Dijkstra T, Haslam E, Meldrum P, Merritt A, Gunn D, Mackay J. (2016). Assessment of ground-based monitoring techniques applied to landslide investigations. *Geomorphology* 253: 438-451.
- Varnes DJ. (1978). *Slope movement types and processes*. In: Schuster RL, Krizek RJ (eds) *Landslides, analysis and control*, special report 176: Transportation research board, National Academy of Sciences, Washington, DC, pp. 11–33.

Outputs and Dissemination

- Brook MS, Merkle J. (2018). Monitoring active landslides in the Auckland region utilising UAV/structure-from-motion photogrammetry. In: RP Orense, M Mimura (Eds.), *International Conference on GIS and Geoinformation Zoning for Disaster Mitigation (GIZ2018)*: 125-130.
- Ryder K, Brook MS, Tunnicliffe J. (2018). Monitoring Mechanisms of Coastal Slope Instability in Auckland, using UAV Photogrammetry data. New Zealand Geographical Society/Australian Institute of Geographers Biennial Conference Auckland, p.122.
- Merkle J, Brook MS, Tunnicliffe J. (2018). Slope failure and engineering geological hazard at Turei Hill, Kawakawa Bay, Auckland. New Zealand Geographical Society/Australian Institute of Geographers Biennial Conference, Auckland, p.96.
- Brook MS, Merkle J. (2019). Monitoring active landslides in the Auckland region utilising UAV/structure-from-motion photogrammetry. *Japanese Geotechnical Society Special Publication* 6(2): 1-6.

Links to publications/theses

- Ryder, K., (2019) *A UAV photogrammetry/DFN modelling approach of analysing rockfall along Auckland's coastal cliffs*. Unpublished Master's thesis, University of Auckland, Auckland, New Zealand.